Eur Biophys J (2003) 32: 544–552
DOI 10.1007/s00249-003-0290-2

ARTICLE

Klaus Winsel · Dirk Hönig · Klaus Lunkenheimer
Katrina Geggel · Christian Witt

Quantitative Brewster angle microscopy of the surface film of human broncho-alveolar lavage fluid

Received: 11 November 2002 / Revised: 4 February 2003 / Accepted: 6 February 2003 / Published online: 25 March 2003

Abstract The morphology, thickness and surface pressure of the surfactant film of broncho-alveoalar lavage (BAL) fluid from patients with sarcoidosis were investigated during spontaneous adsorption of the BAL's surface active material at the air/aqueous buffer interface at 37 °C. The biochemical parameters of the BAL fluid determined were protein (Lowry), total phospholipids (from phosphate after ashing) and the individual phospholipids (HPLC). During the spontaneous adsorption of the pulmonary surfactant the surface pressure increased from initially 26 mN/m to 44 mN/m in the equilibrium state. Simultaneously to the increase of the surface pressure, a continuous increase of the reflectivity signal was observed by quantitative Brewster angle microscopy (BAM). The film thickness is calculated from the reflectivity values using an optical model. The effect of the uncertainty of the refractive index, which has to be estimated, is discussed. The BAM images show the inhomogeneous nature of the surfactant film with three distinct phases of different reflectivity, even at relatively low surface pressures. For the brightest phase, the thickness amounts to approximately 12 nm in the equilibrium state of adsorption. This suggests a multilamellar structure. Additionally, we found visual evidence for an adsorption mechanism involving the spreading of vesicles at the interface, in agreement with published results. Differences in the morphology and thickness of the pulmonary surfactant film reported in the literature are obviously due to the varying experimental conditions and materials. We think that the experimental conditions chosen in our study provide a more realistic view of the structure in the lungs in vivo.

Keywords Brewster angle microscopy · Bronchoalveolar lavage fluid · Lung structure · Pulmonary surfactant · Surface film

K. Winsel (✉) · K. Lunkenheimer · K. Geggel
Independent Research Group, Surfactant Adsorption Layers,
Max-Planck-Institute of Colloids and Interfaces,
Am Mühlberg 1, 14424 Potsdam-Golm, Germany
E-mail: winsel@mpikg-golm.mpg.de
Tel.: +49-0331-5679452
Fax: +49-0331-5679202

D. Hönig
Nanofilm Technology, Göttingen, Germany

C. Witt
Department of Pneumonology, Charitè,
Medical Clinic, Berlin, Germany

Introduction

Bronchoalveolar lavage (BAL) is used in the diagnosis and research of lung diseases in order to isolate and characterize the cellular and fluid components of the lungs (Enzian and Barth 1990; Goldstein et al. 1990; Martin et al. 1990). BAL fluid also contains the surfactant material of the lungs (Goerke 1998) which is responsible for maintaining an appropriate surface tension at the air/alveolar fluid interface during the breathing cycle (Goerke and Clements 1986; Griese 1999).

Phosphatidylcholine, phosphatidylglycerol, phosphatidylethanolamine, sphingomyelin, neutral lipids (e.g. cholesterol) (Creuwel et al. 1997; Veldhusen et al. 1998) and four surfactant associated proteins (SP), SP-A, SP-B, SP-C and SP-D (Pérez-Gil and Keough 1998), are the main components of the surfactant material. Two of the surfactant proteins, probably SP-B and SP-C, are involved in regulating the surface properties, whereas SP-A and SP-D are very important in the infection defence of the lungs (Johansson et al. 1994; Griese 1999).

Concerning the structure of the alveolar lining layer, there are different conceptions. According to a still today widely accepted hypothesis (Clements et al. 1958; Pattle 1958; Brown 1964; Keough 1992), the alveolar lining layer consists of a continuous duplex layer with an aqueous hypophase covered with a monomolecular film of phospholipids, mainly consisting of dipalmitoylphosphatidylcholine. However, the latest results,

especially achieved by scanning force microscopy (SFM) (Amrein et al. 1997; Galla et al. 1998; Grunder et al. 1999), scanning near-field optical microscopy (SNOM) (Kramer et al. 2000), fluorescence light microscopy (FLM) (Amrein et al. 1997; Discher et al. 1999; Krüger et al. 1999) and Brewster angle microscopy (BAM) (Discher et al. 1999) studies, with model mixtures of pulmonary surfactant components, suggest a more complex structure of the pulmonary surfactant film. Depending on the surface pressure, these model films exhibit a pure lipid phase, a protein-enriched lipid phase with aggregates or multilamellar structures designated as protrusions or surface associated reservoirs at higher pressures (Amrein et al. 1997; Galla et al. 1998; Schürch et al. 1998).

Generally, these surfactant model films were spread at the air/aqueous buffer interface from solutions of surfactant proteins and phospholipids in organic solvents. However, some studies suggest that organic solvents and the method of reconstitution alter the surfactant film properties (Cruz et al. 1997; Johansson and Curstedt 1997). On the other hand, the imaging of surfactant film by SFM, SNOM or FLM techniques may also result in some artefacts (Grunder et al. 1999). Using Langmuir-Blodgett transfer of the film from the liquid subphase to solid hydrophilic mica plates, and subsequent drying at room temperature, will most likely drastically change the film structure. In the case of fluorescence methods using fluorescence probes, quenching effects or solubility problems may also occur (Galla et al. 1998).

The direct observation of the pulmonary surfactant or phospholipid film on a liquid phase (in the absence of any fluorescence probe and without transfer of the film onto a solid substrate) by BAM avoids the above-mentioned problems (Hönig and Möbius 1991; Discher et al. 1999).

Phase separation in mixtures of pulmonary phospholipids spread at an air/aqueous buffer interface was demonstrated earlier by BAM (Discher et al. 1999). This technique permits us to visualize separation of the monolayer into domains and a surrounding film with noticeable differences in reflectivity during compression of the film between surface pressures of 20–40 mN/m.

Bronchoalveolar lavage fluid (BAL) represents presumably the most natural material of pulmonary surfactant which can be isolated from the lungs. Therefore, this material resembles the natural state of the surfactant layer more closely than that of any of the artificial films. Only low-speed centrifugation is applied to remove cells and other particular contaminants. These procedures should not influence the molecular structure of the isolated pulmonary surfactant, even though, of course, the lavage procedure itself may change the original biophysical and biochemical microorganization of the pulmonary surfactant system in the lungs in vivo.

The pulmonary surfactant components adsorb very rapidly at the air/water interface, which is suggested to occur via a two-step mechanism (Walters et al. 2000). This process can be followed biophysically by surface tension measurements and structural investigations. In the present work we have studied the changes of structure, thickness and surface pressure of the surfactant film during spontaneous adsorption from the subphase of especially purified BAL fluid by quantitative BAM.

Today, BAM is a well-established method to characterize the morphology of ultrathin films on aqueous subphases. It uses p-polarized light, incident at the Brewster angle of the subphase, depending on its refractive index. Without a surface film, the reflection is ideally zero. In the case when a thin film is present, the refractive index of the film is usually different from that of the subphase, causing a small amount of the incident light to be reflected (typically 10^{-6} for a monolayer of 2 nm thickness). Applying this principle to microscopic observation, one is able to visualize the spatial distribution of the film.

The intensity reflected from a film-covered surface depends on the optical thickness of the film. Growing optical film thickness leads to higher reflected intensity; thus the signal at the Brewster angle contains information about the optical thickness. As shown recently, it is possible to discriminate films of simple, long-chain fatty acids or alcohols which differ by a single carbon atom in their chain length only (Hönig and Möbius 1991). Thus, a resolution on the order of 0.1 nm may be achieved without additional experimental effort.

However, only relatively few reports show the potential of the method to obtain more quantitative results, especially on the thickness of these films (Frey et al. 1996; de Mul and Mann 1998). One reason for this is due to the fact that the measurement is a photometric one[1], requiring a precise calibration of the instrument that allows one to recalculate the gray values of the image in terms of reflectivity. We will describe a simple method to perform this calibration later.

Another reason is that optical methods applied to ultrathin films (< 20 nm) can usually not determine the film thickness without estimating the refractive index of the material, as it is practically impossible to decouple the two quantities. However, it is possible to use a certain reasonable range of the refractive index, which will be close to the value of the bulk material (for non-absorbing materials). Taking the uncertainty in the refractive index of the optical modelling into account results in an error for the thickness which is acceptable in many cases. A simple optical model that can be applied is a single-layer model based on Fresnel's equation (Azzam and Bashara 1987). Using the special geometrical relations at the Brewster angle and applying a thin film approximation, one can further simplify the model[2]

[1] An example of a non-photometric measurement is the nulling ellipsometry which measures the rotation angles of optical elements at a signal minimum. In this case the absolute magnitude of the signal is not important

[2] The approximation may be easily derived using (1) the trigonometric relations following from the fact that, at the Brewster angle, reflected and refracted beams are perpendicular, (2) Brewster' s law and (3) a thin film approximation where the thickness of the film is small compared to the wavelength

to derive a simple equation for the reflectivity R of a thin, single-layered film:

$$R = \frac{I_r}{I_0} = \left(\pi \frac{d}{\lambda}\right)^2 \frac{\left(n_1^2 - n_2^2 - 1 + n_2^2/n_1^2\right)^2}{1 + n_2^2} \quad (1)$$

where I_0 and I_r denote the incident and the reflected intensity, respectively, $n_{1,2}$ is the refractive index of the film (1) and/or of the subphase (2), λ is the wavelength of the incident light and d is the thickness of the film.

When it is expected that the refractive index is rather constant during the process to be observed, valuable, semi-quantitative information can be obtained even though the refractive index is not known precisely.

Additional problems of optical modelling can occur due to the intrinsic, highly ordered nature of the monomolecular layers. This may cause optical anisotropy, which is often observed in BAM imaging as a contrast between domains of different orientation, especially when a second polarizer in front of the camera operates as an analyzer to distinguish different polarization states of the detected light. It is sometimes possible to obtain additional structural information (tilt angle, domain orientation) from such images, using more refined optical models for anisotropic layers (Overbeck et al. 1994). For many types of films, however, such anisotropy is not observed and it is then justified to assign a certain single value to the refractive index. This is true in particular for many films of complex mixtures of different molecular species, because the mixing usually hinders the formation of highly ordered phases.

Setting the analyzer (A) of the Brewster angle microscope close to the ''crossed polarizers'' position (i.e. at $A = 90°$ with respect to the plane of incidence), it is easily possible to identify a film as optically isotropic or anisotropic (except for the special case of a purely uniaxially anisotropic film where the anisotropy axis is vertical). The isotropic film will cause the reflected light to be purely p-polarized (if the polarizer P is set exactly to p-position $P = 0°$). Thus, the image will appear dark for $A = 90°$. An anisotropic film would cause the reflected light to contain some s-polarized component reaching the camera, and especially an inversion of contrast between domains of different in-plane orientation would be observed when swinging the analyzer to symmetric positions on both sides of $A = 90°$ (e.g. $A = 90 \pm 20°$).

Thus, to be able to use BAM for the measurement of the film thickness of isotropic films, the following conditions are required:

1. A photometrically calibrated Brewster angle microscope with a digital image processing system to obtain gray level information on selected areas of the image.
2. Isotropic films or films with negligible anisotropy which can be tested by the procedure described above.
3. Reasonable estimates of the refractive index of the film.

Material and methods

Materials

Folin-Ciocalteu's reagent, human albumin, BHT (butylated hydroxytoluene), L-α-phosphatidylethanolamine from egg yolk, L-α-phosphatidyl-DL-glycerol ammonium salt, L-α- phosphatidylinositol sodium salt from soybean, dipalmitoyl-DL-α-phosphatidylcholine (C16:0), L-α-phosphatidylserine from bovine and sphingomyelin from chicken egg yolk were obtained from Sigma, Germany.

Chloroform, methanol, water (all HPLC grade), ammonium hydroxide solution (25%), amidol (2,4-diaminophenol hydrochloride, purum) and ammonium molybdate p.a. were obtained from Fluka, Switzerland. H_2SO4 p.a., HNO_3 p.a. and KH_2PO4 p.a. were purchased from Merck, Germany. Sodium hydrogensulfite solution (38–40%) was from Riedel-de-Haen, Germany.

Methods

Bronchoalveolar lavage

BAL was performed by fiberoptic bronchoscopy under premedication with hydrocodan, atropine and imidazolam and local anesthesia with prilocaine in the middle lobe within the framework of the clinical diagnosis of lung diseases. Patients with the diagnosis sarcoidosis were included in the study. BAL was performed after patients' written consent and BAL was in agreement with the local ethics committee (Charitè, Berlin).

Both 5×20 mL and 1×10 mL of isoosmotic saline were instilled through the working channel of the bronchoscope with a syringe and aspirated immediately after instillation (total recovery about 65%). The first fraction was used for microbiological investigations and the following fractions were pooled in an ice-cold siliconized glass vessel. The BAL fluid was then filtered through a sterile gauze and centrifuged at 400×g and 4 °C for 10 min to remove mucus and cells, respectively. The supernatant was used for the investigations.

The BAL fluids of these patients were pooled to sufficient amounts in order to average the surfactant concentrations in the BAL fluids of different patients. All investigations were performed with averaged samples. The BAL pool was stored at −70 °C. Immediately before use the frozen BAL fluid was thawed at room temperature and centrifuged again at 400×g and 4 °C.

Protein determination

The protein concentration in the BAL fluid was measured by the Lowry method (Lowry et al. 1951). The assay was performed with 0.5 mL of BAL fluid using 12 dilutions of human albumin containing concentrations from 10 to 1000 μg/mL as standards. The calibration curve was plotted by linear regression analysis ($R^2 > 0.99$). The mean values ± SD of three separate determinations were calculated.

Extraction of the lipids from BAL fluid

The lipids were extracted by the Folch method (Folch et al. 1957), with small modifications. In brief, 10 mL of the cell-free lavage fluid were mixed with 40 mL of chloroform/methanol (2:1, v/v) containing 0.1% BHT in a separatory funnel and shaken for 5 min. After 10 min of standing, the lower lipid-containing phase was separated and washed with 2 mL of the pure solvent upper phase (Folch et al. 1957). Thereafter, the lower phase was separated, centrifuged and dried under a nitrogen stream at room temperature. The residue was dissolved immediately in 500 μL mobile phase A for the HPLC separation or used for the total

phospholipid determination. The samples were stored in a glass tube with a screw cap at −70 °C prior to the analysis.

Total phospholipid determination

The dried lipid extract of 10 mL BAL fluid was digested with 300 μL conc. H_2SO4 and 100 μL conc. HNO_3 at 350 °C. After 10 min of heating, 50 μL HNO_3 were once more added and the solution was heated again until a white vapor was visible. The residue was diluted with distilled water (1:25) and the phosphate concentration was determined by the Allen method (Allen 1940) using amidol as reducing agent. For the phosphate calibration curve, 11 dilutions of pure KH_2PO4 (5–75 μg PO_4^{3-}/mL) were used. Regression line analysis was performed for fitting of the calibration curve ($R^2 > 0.99$). For the calculation of the total phospholipids from phosphate, a factor 8.16 was applied. Three separate determinations were done and the results are given as mean values ± SD.

HPLC of the surfactant phospholipids

HPLC was performed with a Shimadzu high-performance liquid chromatograph fitted with a system controller (SCL-10 A vp), a diode array (SPD-M-10 A vp), a UV detector (SPD-10 A vp), a pump (LC-10 AD vp), a gradient mixer (FCV-10 AL vp) and a light-scattering detector (ELSD 500, Alltech, Germany).

The separation of the surfactant phospholipids was performed according to Bünger and Pison (1995). A guard (20×2.1 mm ID) and an analytical column (120×4.6 mm ID) packed with Encapharm, a spherical silica gel with stability up to pH 10 (5 μm particle size, 10 nm pore size and 320 m^2 /g surface area), were used (Molnar, Berlin, Germany).

The mobile phase consisted of 80% chloroform, 19.5% methanol and 0.5% ammonium hydroxide (25%) (solvent A) and 60% chloroform, 34% methanol, 5.5% water and 0.5% ammonium hydroxide (25%) (solvent B). The linear gradient had the following course: from 0 to 100% B within 14 min, followed by 9 min at 100% B, then down to 0% B within 7 min and finally 10 min at 0% B.

Between the single runs, one or two empty solvent gradients were applied. The flow rate was 1 mL/min. The temperature of the light-scattering detector was set at 50.3 °C. The nebulizer of the light-scattering detector was run with a flow rate of 1.70 mL/min of pure nitrogen.

The quantitative data were obtained from the calibration curves (area/μg/mL) for the single phospholipids. The calibration curves were obtained by six different concentrations of each phospholipid in the range 25–200 μg/mL and fitted by linear regression analysis ($R^2 > 0.99$). Three separate runs were performed and the mean values ± SD calculated.

Calibration of the Brewster angle microscope

The photometrical calibration of a Brewster angle microscope provides us with the calibration curve that correlates the measured brightness of the image (usually provided as the gray level by a digital image-processing system) and the reflectivity of the sample, i.e. the ratio of reflected and incident illumination intensity. Since the light distribution in a BAM image is usually not very homogeneous, due to the direct imaging of a small diameter laser beam, it is important to perform calibration and measurement on the same region of the image, to keep the illumination level constant. To increase the signal-to-noise ratio, it is recommended to average the signal over an extended region of the image instead of taking the gray level value of a single image pixel. At the air/water interface, this requires keeping the water level constant with respect to the microscope to avoid shifts of the laser beam due to evaporation. Of course, the light source itself must also be stable in time. After calibration of the instrument, changes of the optical configuration or of the camera were allowed only if the effect on the measured intensity was well known. For example, changing the exposure time (''electronic shutter'') of the CCD camera has a reproducible and quantitatively known effect on the signal.[3]

The calibration described here uses the fact that the reflected intensity generated by the pure, clean water surface when the angle of incidence is slightly shifted away from the Brewster angle is well known from the Fresnel equation for the reflection of a p-polarized light beam from the surface. When passing the Brewster angle, the camera signal reaches a minimum. The signal as a function of the incidence angle is approximately described by a parabola in the close vicinity of the minimum (Fig. 1a). To achieve saturation of the camera, an angle range of only a few tenths of a degree around the minimum will be enough for a typical BAM measurement. Saturation of the camera has to be avoided on all pixels that are used for the calibration.

In the first step, fitting a parabola to the curve allows one to precisely obtain the position of the Brewster angle, which can differ from the actual display (if the instrument shows the angle) by a small amount due to alignment tolerances of the instrument or other error sources. Comparison of the measured and the theoretically expected Brewster angle $\phi_B = \arctan(n_2)$ gives the offset to correct the x-axis of the plot.

Using Fresnel's reflection coefficient for p-polarized light (Azzam and Bashara 1987), we can calculate the theoretically expected reflectivity of the clean subphase for the set of angles of incidence used for the calibration. Plotting the theoretical reflectivity R against the measured intensity G (in gray levels), we obtain the linear calibration curve of R versus G, provided that the response of the camera is linear.[4] A linear regression easily gives the background signal at the Brewster angle and the slope, thus providing the quantities needed to obtain the reflectivity from a given gray level (Fig. 1b).

Visualization of the surface film by BAM and measurement of the surface pressure

The structure of the pulmonary surfactant adsorption layer from BAL fluid was visualized with a Brewster angle microscope (BAM 2 plus) equipped with a high-power green laser (50 mW at 532 nm) (Nanofilm Technology, Göttingen, Germany).

The microscope was placed at the center of a Langmuir minitrough. The trough was positioned on a lift, allowing it to be raised up and down. The fine tuning of the vertical position of the microscope was done with the instrument's vertical lift. The polarizer P and the analyzer A were both set to 0°. The stored images were processed with dedicated image processing functions.

Experiments were performed with a NIMA Langmuir minitrough 601M (7×15 cm; 105 cm^2) with symmetric compression (NIMA, Coventry, UK). The surface pressure was recorded with a PS4 pressure sensor using Wilhelmy plates consisting of filter paper. The NIMA trough was connected with a thermostat and tempered at 37 °C. The preheated BAL fluid was poured into the Langmuir trough (approx. 52 mL). The barriers were opened to the maximum trough area after aspiration of the surface to remove the initial surface film.

Thereafter, the spontaneous formation of the surfactant film was observed by BAM. Parallel to the monitoring of the surface pressure, the gray level G is recorded by averaging the signal in a central region-of-interest (same as used for the calibration). Small local defects or particles which might be produced by aggregation or by instabilities of the interfacial layer were not taken into account, as only homogeneous film areas produce a reliable G signal. Therefore, the region of interest within the image used for the signal generation was sized to approx. 50×50 μm^2, which

[3]Special care has to be taken with the background signal of the camera when no light is present, as this ''black level'' will not be scaled in the same way as the light signal when the exposure time changes

[4]A non-linear response, e.g. at high brightness levels, would result in a deviation from the linear curve

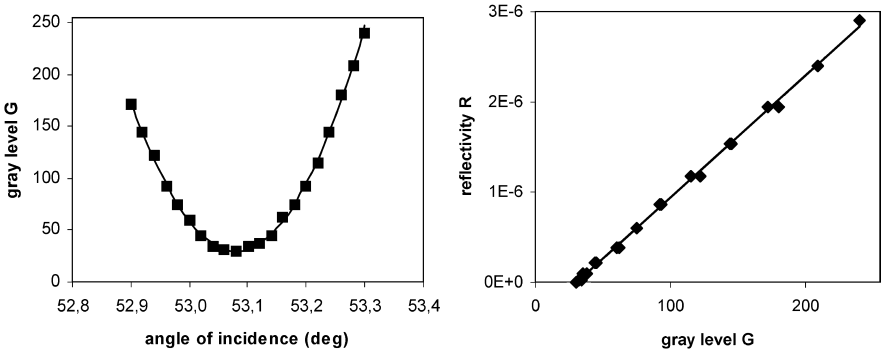

Fig. 1 *Left*: gray levels measured in the vicinity of the Brewster angle for the clean water subphase. The angle of incidence is slightly altered, producing the shown gray levels with a digital image processing system. *Right*: the calibration curve *R* versus G (reflectivity as a function of the gray level) obtained by applying the described calibration procedure

Table 1 Protein and phosholipid concentrations (μg/mL) of human bronchoalveolar lavage fluid[a,b]

Protein	Total phospholipid	PG	PE	PI	PC
242.3 ± 3.21	20.56 ± 0.57	2.09 ± 0.11	1.77 ± 0.01	1.63 ± 0.08	14.75 ± 0.93

[a]PG = L-α-phosphatidylglycerol, PE = L-α-phosphatidylethanolamine, PI = L-α-phosphatidylinositol, PC = DL-α-phosphatidylcholine
[b]Mean ± SD values of three different determinations are given

proved to be large enough to average out local film inhomogeneities.

From time to time, BAM images of typical film states were taken. Gray level data from these (unprocessed) images complement the continuous recording of *G* for particularly interesting film structures.

The surfactant film is floating due to thermal convection and surface pressure gradients. Thus, the *G* signal is strongly fluctuating due to the inhomogeneous nature of the film, as areas of different brightness are passing the region-of-interest. In particular, the signal is changing between nearly the background signal for the areas that are covered with a very thin film, and for the brightest domains.

To extend the dynamic range of the instrument, we operated the camera at different exposure times: as soon as the *G* signal was reaching almost saturation of the camera, we switched to a lower sensitivity by decreasing the exposure time. This procedure changes the sensitivity in a well-defined way, keeping the calibration unaltered. The raw data of the *G* signal were in the range 0–255, using an 8-bit frame grabber. Using exposure times of 1/250, 1/500, 1/1000, 1/2000 and 1/5000 s, we could extend the available virtual gray scale from 0 to 5100, allowing us to measure the initial, thin surfactant film at the beginning of the experiment as well as the very bright domains of the surfactant film in the final state of spontaneous adsorption.[5]

Results

Biochemical composition of the BAL components

In order to characterize the surface active compounds of the BAL fluid, the total phospholipids, the single phospholipids and the total protein concentration were determined. The data are given in Table 1.

[5]The gray level resolution of the camera is *not* changed by a factor of 20 in this way. For each setting of the exposure time, *G* still has 8-bit resolution

Reflectivity curve and surface pressure of the surface film

Figure 2 shows a reflectivity curve obtained in the way described above from the *G* signal by using the calibration parameters. The solid line is an approximation corresponding to the brightest domains, representing the increase in thickness of a part of the surfactant film. Just after starting the measurement, the reflectivity already showed a non-zero value, caused by the fact that a thin surfactant film was forming nearly instantaneously. The film reached a saturated state after approximately one hour. After this time, the film structure, the surface pressure and the maximum reflectivities did not show significant changes.

The drop of the lower limiting values of the reflectivity is caused by the fact that, even in the saturated film state, a significant amount of the surface is covered by relatively thin film. These particular film areas do not significantly contribute to the *G* signal at the low exposure time required for the high-brightness domains of the saturated film state.

The surface pressure of the surfactant film increases during the adsorption from approximately 26 mN/m to 44 mN/m. The maximum reflectivity and the film surface pressure show a similar development with time.

Imaging of the surface film by BAM

The inhomogeneous nature of the pulmonary surfactant film is known from previous work (Amrein et al. 1997; Galla et al. 1998; Discher et al. 1999; Grunder et al. 1999; Krüger et al. 1999; Kramer et al. 2000). The BAM images of this film reveal some interesting features, as shown in Fig. 3. The images correspond to the concerned regimes of the reflectivity and the surface pressure curve, as shown in Fig. 2. Please note that the relative brightness of the

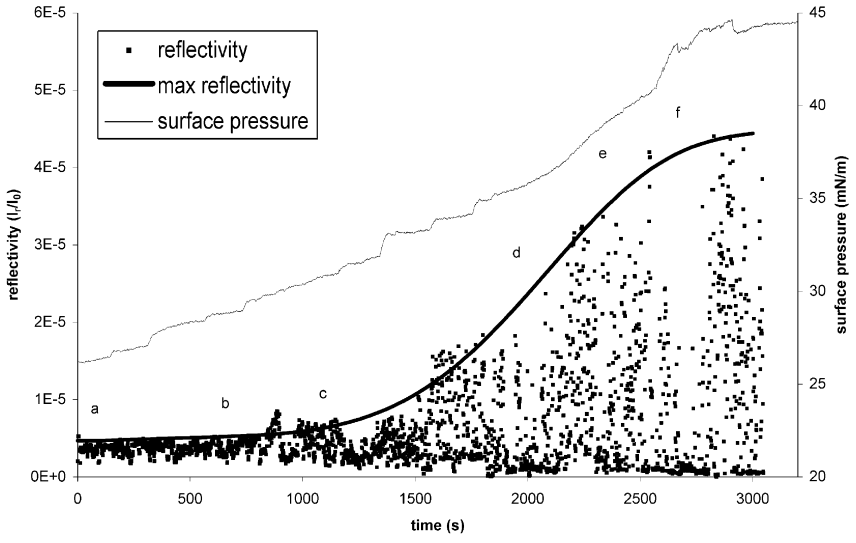

Fig. 2 Reflectivity and the surface pressure measured during the spontaneous formation of the surfactant film. The *solid line* of the reflectivity curve represents the maximum values of the brightest domains at each film state. *Alphabetic markers* on the curve correspond to the images in Fig. 3

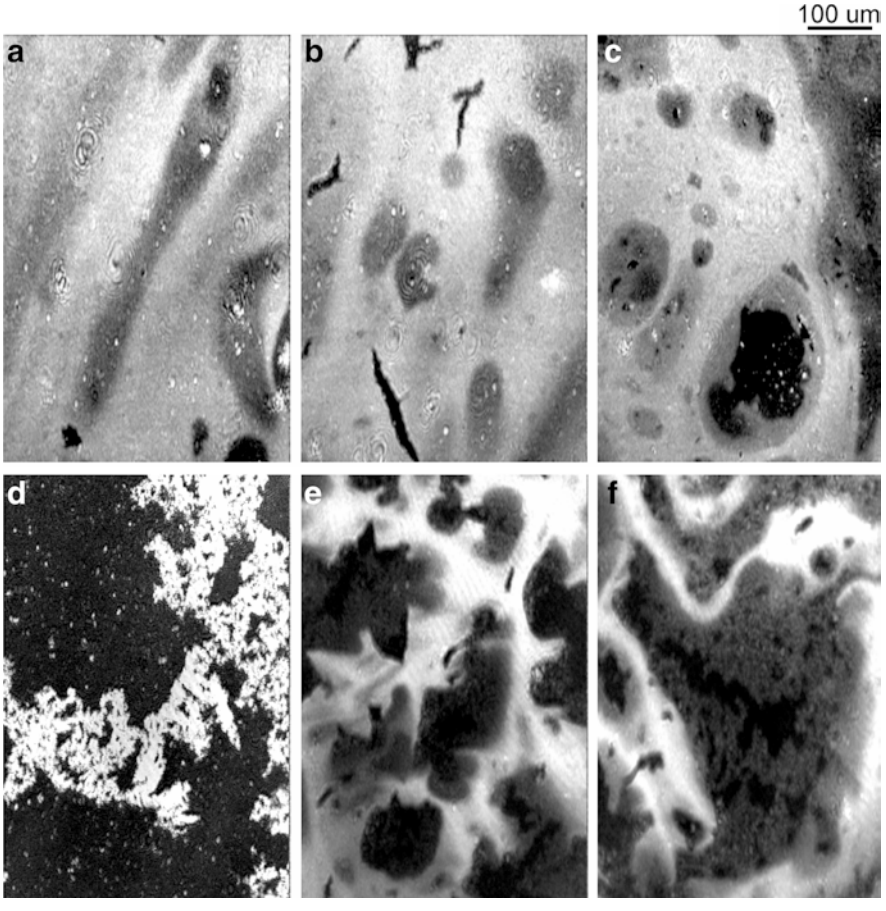

Fig. 3 BAM images at different states of the surfactant films during spontaneous adsorption from the subphase at the air/isoosmotic saline interface. The surface pressures and the corresponding exposure times amount to (**a**) 26 mN/m, 1/250 s; (**b**) 29 mN/m, 1/250 s; (**c**) 32 mN/m, 1/500 s; (**d**) 32 mN/m, 1/2000 s; (**e**) 38 mN/m, 1/2000 s; and (**f**) 44 mN/m, 1/5000 s. See text for details

images are influenced by the different exposure times used during the experiment. Figure 3f has approximately 10–20 times higher reflectivity than Fig. 3a.

In the beginning (Fig. 3a), at a surface pressure of approximately 26 mN/m, the inhomogeneous surfactant film is strongly floating. The domains are bending due to this motion, producing soft domain boarders, indicating already a certain gradient of thickness or density. On increasing the surface pressure to about 29 mN/m, the film becomes more rigid. This can be seen in Fig. 3b in the form of ''cracks'' with sharp-edged borders. At a later stage of the surfactant layer, distinctly differing phases are observed. The films show clearly separated areas of different brightness. In Fig. 3c, at approximately

32 mN/m, one can discriminate three film areas of different thickness corresponding to a dark, an intermediate and a bright phase. The sharp borders of these phases indicate that they presumably consist of molecular species of different lipid-protein composition. Therefore the BAM images clearly demonstrate three different phases of the surface morphology.

Owing to the strongly inhomogeneous nature of the monolayer and of the complex mixture, the film sometimes shows structures of different morphology. As might be expected for biological material, it is sometimes not quite clear to assign a specific surface structure to the surfactant film or to an artefact, like for the structure in Fig. 3d. On the other hand, similar structures have been described as protein-enriched phases with protein aggregations (Kramer et al. 2000).

The surfactant film reaches its final state in Fig. 3e and Fig. 3f, at a surface pressure of about 44 mN/m, showing typical web-like structures. Most pronounced is the fact that the film does not exhibit a homogeneous brightness, but has still a strongly inhomogeneous domain structure. As in Fig. 3c, three different phases are still clearly separated, where the brightest phase, corresponding to the highest reflectivity levels in Fig. 2, shows some brightness gradients which have to be interpreted as thickness gradients.

By making use of the instrument's analyzer, we checked that the film exhibited no significant optical anisotropy, allowing us to use the simple optical model described above.

Modelling of the film thickness

The film thickness can be derived from the images or the reflectivity curve by solving the single-layer reflectivity equation (Eq. 1) for the thickness d. The required parameters are $n_2 = 1.333$ (refractive index of the subphase) and $\lambda = 532$ nm (wavelength of the light source).

For the unknown refractive index n_1 of the film, we have to use an estimation. A reasonable range for biological material is $n = 1.43$–1.47 in the visible range. This range already leads to a relatively large uncertainty for the calculated thickness of about $\pm 25\%$ of the mean value. However, the main consequences are not influenced.

Plots of the obtained thickness of the brightest domain are given in Fig. 4 for three different estimations of the refractive index. Immediately after the beginning of the adsorption the surface film has a thickness of approximately 3.7 nm ($\pm 25\%$). It is interesting that this value is almost identical to the thickness of a bilayer. At the equilibrium state of the adsorption process, the surfactant film thickness of the brightest domains increases to approximately 11.5 nm ($\pm 25\%$).

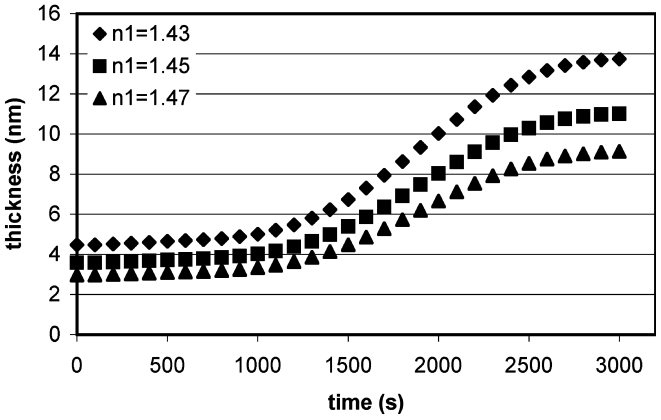

Fig. 4 Thickness development of the brightest domains in dependence on time during spontaneous adsorption of the BAL surfactant layer. Given are three curves of different estimated refractive index values. The uncertainty in the refractive index leads to about $\pm 25\%$ variation of the calculated thickness

Discussion

Measurement of the surface pressure of the film indicates that the air/liquid interface contains a high concentration of surface active components of the pulmonary surfactant, which increases continuously during the adsorption. The rise of the surface pressure is accompanied by a continuous increase of the thickness of a part of the surfactant film, suggesting the incorporation of surface active material from the bulk phase into the film.

The mechanism of the film formation is partly revealed by the BAM images. Frequently one can observe a "particle" approaching the surface from the subphase. In the moment of appearance of the particle at the interface, a spherical domain of film is forming in a very rapid way. This behaviour may be explained as the spreading of a monolayer from a vesicle that is decaying at the interface. These results are in agreement with the investigations of another group, which found distinct steps in the adsorption of pulmonary surfactant to the air/liquid interface (Walters et al. 2000). According to the conclusions of that group, vesicles approach the interface in a first step and then fuse with the interface in a second step.

Taking into account the results obtained with other techniques of surfactant film imaging (Amrein et al. 1997; Galla et al. 1998; Discher et al. 1999; Grunder et al. 1999; Krüger et al. 1999; Kramer et al. 2000), the three different phases of the surface film may be attributed to a pure lipid phase, a protein-enriched lipid phase and multilamellar structures of lipids and proteins, representing the postulated protrusions or the surface associated reservoirs. This is in agreement with our results presented here. We observed three coexisting phases even at high surface pressures of 44 mN/m. Surface structures of about 12 nm thickness are found using quantitative BAM. This thickness is much greater than the value of one single monolayer (2 nm), a DPPC bilayer (about 5 nm) (Amrein et al. 1997) or a single protrusion stack (6.0–6.5 nm) (Galla et al. 1998). Therefore, multilayer structures formed in these brightest domains are suggested.

Multiple-stacked protrusions of 28 nm and/or 77 nm thickness of compressed SP-C containing model surfactant films (at surface pressures of about 50 mN/m), which are compatible with the formation of multilayers, were recently demonstrated by SFM investigations (Amrein et al. 1997; von Nahmen et al. 1997; Grunder et al. 1999). However, another group was unable to detect protrusions in compressed model surfactant films at surface pressures of about 40 mN/m by SFM (Grunder et al. 1999). Additionally, the morphology of the surfactant film as shown by BAM and SFM (Amrein et al. 1997, fig. 4a) are quite different.

There are many possible reasons for the deviating results of the works published in this field. Certainly, different surface pressures may lead to various structures of the surface film. However, it is most likely that differences in the kind of surfactant material and the various techniques of preparation applied are responsible. Most important is presumably the fact that the surfactant film cannot be investigated by SFM in situ or on an aqueous subphase. The transfer of the surfactant film onto a solid substrate by the LB technique will most certainly be affected by heavy artefacts. In contrast to that, in our investigation the pulmonary surfactant films were formed from almost native surfactant material during spontaneous adsorption and imaged with BAM without further manipulations.

We think that owing to the use of carefully treated, native BAL fluid and the application of the non-interfering BAM technique to the BAL adsorption layers, the observed structures provide a more realistic picture of the morphology of pulmonary surfactant film in vivo in comparison to that gained with other techniques.

Acknowledgements This work was supported by a grant from the Bundesministerium für Bildung und Forschung (project number: 13N7283/0).

References

Allen R (1940) The estimation of phosphorus. Biochem J 34:858–862

Amrein M, von Nahmen A, Sieber M (1997) A scanning force- and fluorescence light microscopy study of the structure and function of a model pulmonary surfactant. Eur Biophys J 26:349–357

Azzam RMA, Bashara NM (1987) Ellipsometry and polarized light. North-Holland, Amsterdam

Brown ES (1964) Isolation and assay of dipalmitoyl lecithin in lung extracts. Am J Physiol 207:402–406

Bünger H, Pison U (1995) Quantitative analysis of pulmonary surfactant phospholipids by high-performance liquid chromatography and light-scattering detection. J Chromatogr B 672:25–31

Clements JA, Brown ES, Johnson R (1958) Pulmonary surface tension and the mucus lining of the lung: some theoretical considerations. J Appl Physiol 12:262–268

Creuwel LAJM, van Golde LMG, Hangsman HP (1997) The pulmonary surfactant system: biochemical and clinical aspects. Lung 175:1–39

Cruz A, Casals C, Keough KMW, Pérez-Gil J (1997) Different modes of interaction of pulmonary surfactant protein SP-B in phosphatidylcholine bilayers. Biochem J 327:133–138

de Mul MNG, Mann JA (1998) Determination of the thickness and optical properties of a Langmuir film from the domain morphology by Brewster angle microscopy. Langmuir 14:2455–2466

Discher BM, Schief WR, Vogel V, Hall SB (1999) Phase separation in monolayers of pulmonary surfactant phospholipids at the air-water interface: composition and structure. Biophys J 77:2051–2061

Enzian P, Barth J (1990) Bronchoalveolar lavage. Dtsch Med Wochenschr 115:663–666

Folch J, Lees M, Stanlay GHS (1957) A simple method for the isolation and purification of total lipids from animal tissue. J Biol Chem 226:497–509

Frey W, Schief WR, Vogel V (1996) Two dimensional crystallization of streptavidin studied by quantitative Brewster angle microscopy. Langmuir 12:1312–1320

Galla HJ, Bourdos N, von Nahmen A, Amrein M, Sieber M (1998) The role of pulmonary protein C during the breathing cycle. Thin Solid Films 327–329:632–635

Goerke J (1998) Pulmonary surfactant: functions and molecular composition. Biochim Biophys Acta 1408:79–89

Goerke J, Clements JA (1986) Alveolar surface tension and lung surfactant. In: Fishman AP (ed) Handbook of physiology, section 3: the respiratory system, vol. III, part 1. American Physiological Society, Bethesda, Md., pp 247–261

Goldstein RA, Rohatgi PK, Bergofsky EH, Block ER, Daniele RP, Dantzker DR, Davis GS, Hunnighake GW, King TE Jr, Metzger WJ (1990) Clinical role of bronchoalveolar lavage in adults with pulmonary disease [see comments]. Am Rev Respir Dis 142:481–486

Griese M (1999) Pulmonary surfactant in health and human lung diseases: state of the art. Eur Respir J 13:1455–1476

Grunder R, Gehr P, Bachofen H, Schürch S, Siegenthaler H (1999) Structures of surfactant films: a scanning force microscopy study. Eur Respir J 14:1290–1296

Hönig D, Möbius D (1991) Direct visualization of monolayers at air-water interface by Brewster angle microscopy. J Phys Chem 95:4590–4592

Johansson J, Curstedt T (1997) Molecular structures and interactions of pulmonary surfactant components. Eur J Biochem 244:675–693

Johansson J, Curstedt T, Robertson B (1994) The proteins of the surfactant system. Eur Respir J 7:372–391

Keough KMW (1992) Physical chemistry of pulmonary surfactant in the terminal air spaces. In: Robertson B, van Golde LMG, Batenburg JJ (eds) Pulmonary surfactant: from molecular biology to clinical practice. Elsevier, Amsterdam, pp 109–164

Kramer A, Wintergarten A, Sieber M, Galla HJ, Amrein M, Guckenberger R (2000) Distribution of the surfactant-associated protein C within a lung surfactant model film investigated by near-field optical microscopy. Biophys J 78:458–465

Krüger P, Schalke M, Wang Z, Notter RH, Dluhy RA, Lösche M (1999) Effect of hydrophobic surfactant peptides SP-B and SP-C on binary phospholipid monolayers. I. Fluorescence and dark field microscopy. Biophys J 77:903–914

Lowry OH, Rosebrough NJ, Farr AL, Randall RJ (1951) Protein measurement with the Folin phenol reagent. J Biol Chem 193:265–275

Martin WR, Padrid PA, Cross CE (1990) Bronchoalveolar lavage. Clin Rev Allergy 8:305–332

Overbeck GA, Hönig D, Möbius D (1994) Stars, stripes and shells in monolayers: simulation of the molecular arrangement in Schlieren structures. Thin Solid Films 242:213–219

Pattle RE (1958) Properties, function, and origin of the alveolar lining layer. Proc R Soc London Ser B 148:2176–240

Pérez-Gil J, Keough MW (1998) Interfacial properties of surfactant proteins. Biochim Biophys Acta 1408:203–217

Schürch S, Green FHY, Bachofen H (1998) Formation and structure of the surface film: captive bubble surfactometry. Biochim Biophys Acta 1408:180–202

Veldhusen R, Nag K, Orgeig S, Possmayer F (1998) The role of lipids in pulmonary surfactant. Biochim Biophys Acta 1408:90–108

von Nahmen A, Schenk M, Sieber M, Amrein M (1997) The structure of a model pulmonary surfactant as revealed by scanning force microscopy. Biophys J 72:463–469

Walters RW, Jeng RR, Hall SB (2000) Distinct steps in the adsorption of pulmonary surfactant to an air-liquid interface. Biophys J 78:257–266